State of Oregon
Oregon Department of Geology and Mineral Industries
Vicki S. McConnell, State Geologist

OPEN-FILE REPORT O-13-19

TSUNAMI INUNDATION SCENARIOS FOR OREGON

by George R. Priest[1], Robert C. Witter[2], Y. Joseph Zhang[3], Kelin Wang[4], Chris Goldfinger[5], Laura L. Stimely[1], John T. English[6], Sean G. Pickner[7], Kaleena L.B. Hughes[7], Taylore E. Wille[7], and Rachel L. Smith[7]

2013

[1]Oregon Department of Geology and Mineral Industries, Coastal Field Office, 313 SW 2nd Street, Suite D, Newport, OR 97365
[2]U.S. Geological Survey, Alaska Science Center, 4210 University Dr., Anchorage, AK 99508
[3]Virginia Institute of Marine Science, Center for Coastal Resources Management, 1375 Greate Road, P.O. Box 1346, Gloucester Point, VA 23062
[4]Geological Survey of Canada, Pacific Geoscience Centre, Room 4714m, 9860 West Saanich Road, Sidney, British Columbia, Canada V8L 4B2
[5]College of Earth, Ocean and Atmospheric Sciences, Oregon State University, Ocean Admin. Bldg. 104, Corvallis, OR 97331
[6]City of Hillsboro, Information Services, Civic Center 150 E. Main Street, Hillsboro, OR 97123
[7]Oregon Department of Geology and Mineral Industries, 800 NE Oregon Street, #28, Suite 965, Portland, OR 97232

NOTICE

This product is for informational purposes and may not have been prepared for or be suitable for legal, engineering, or surveying purposes. Users of this information should review or consult the primary data and information sources to ascertain the usability of the information. This publication cannot substitute for site specific investigations by qualified practitioners. Site specific data may give results that differ from the results shown in the publication.

Oregon Department of Geology and Mineral Industries Open-File Report O-13-19
Published in conformance with ORS 516.030

For copies of this publication or other information about Oregon's geology and natural resources, contact:

Nature of the Northwest Information Center
800 NE Oregon Street #28, Suite 965
Portland, Oregon 97232
(971) 673-2331
http://www.naturenw.org

For additional information:
Administrative Offices
800 NE Oregon Street #28, Suite 965
Portland, OR 97232
Telephone (971) 673-1555
Fax (971) 673-1562
http://www.oregongeology.org
http://egov.oregon.gov/DOGAMI/

TABLE OF CONTENTS

LIST OF TABLES

LIST OF FIGURES

ABSTRACT

This digital data release is for seven tsunami inundation scenarios for the entire Oregon coast in the form of polygons (Esri ArcGIS® shapefiles). These scenarios are depicted on published Oregon Department of Geology and Mineral Industries (DOGAMI) tsunami inundation maps (TIM series). The hydrodynamic computer model SELFE is used to simulate tsunami generation, propagation and maximum inundation for five Cascadia subduction zone (CSZ) earthquake sources (SM1, M1, L1, XL1, XXL1) and two M_w (moment magnitude) 9.2 Alaska earthquake sources: the historical maximum that struck in 1964 (AK64) and a hypothetical maximum (AKMax) with highly efficient focusing of tsunami energy at the Oregon coast. Inundation for XXL1 and the AKMax are the recommended evacuation zones for local and distant tsunamis, respectively. Model CSZ slip is estimated primarily from size and time between deposits left behind by submarine sand and silt slurries (turbidites) triggered by CSZ earthquakes. Relative CSZ tsunami heights at each latitude scale directly to local peak fault slip calculated from model time intervals over which the CSZ accumulates slip that is released in earthquakes as follows: Sm1 = 300 yrs, M1 = 425-525 yrs, L1 = 650–800 yrs, XL1 = 1,050–1,200 yrs, XXL1 = 1,200 yrs. All five CSZ sources partition fault slip from the CSZ megathrust to an offshore splay fault with an average eastward inclination of ~30°. Based on a logic tree summarizing sources of variability, the five CSZ inundations cover the following percentages of potential variability in CSZ tsunami inundation: Sm1 = 26%, M1 = 79%, L1 = 95%, XL1 = 98%, and XXL1 = 100%. Model tide for all seven scenarios is assumed to be mean higher high water (MHHW), varying south to north from 2.07 m to 2.71 m NAVD88 (North American Vertical Datum of 1988). Tsunami simulations use unstructured computational grids constructed from detailed bathymetric and topographic data, particularly lidar. Spacing between computational grid points, a measure of the precision of the inundation boundaries, is generally less than 10 m in populated areas and at critical shoreline features such as jetties.

INTRODUCTION

The intent of this digital data release is to provide seamless, statewide tsunami inundation scenarios in the form of Esri® ArcGIS® shapefiles for seven scenarios selected for depiction on published Oregon Department of Geology and Mineral Industries (DOGAMI) tsunami inundation maps (TIM series). These scenarios include five from local Cascadia subduction zone (CSZ) earthquakes (SM1, M1, L1, XL1, and XXL1) and two maximum-considered distant tsunamis from subduction zone earthquakes in the Gulf of Alaska: a historical maximum that occurred in 1964 (AK64) and a hypothetical maximum (AKMax) with higher uplift and more efficient focusing of tsunami energy at the Oregon coast than in 1964. This paper provides a brief technical summary of the tsunami mapping approach, but see Witter and others (2011) for detailed information on how the Cascadia scenarios were developed and tested against geological, geophysical, and paleoseismological observational data. See Priest and others (2009, 2010) and Witter and others (2011) for details of Alaska scenarios. Table 1 summarizes key parameters for each earthquake source. Results of Cascadia fault rupture and tsunami simulations are summarized in Table 2. All simulations were run at the tidal levels and other input parameters listed in Table 3.

Table 1. Estimated earthquake parameters for tsunami source scenarios used in Oregon tsunami inundation maps (TIM series).

Rupture Scenario (Witter and others, 2011)	Tsunami Inundation Map (TIM Series) Scenario	Length (km)	Width (km)[a]	Slip Deficit Time (years)	Maximum Slip (m)[b]	Average Slip (m)[c]	Moment Magnitude (M_w)[d]
XXL1	XXL	1,000	83	1,200	41	20	9.1
XL1	XL	1,000	83	1,050–1,200	41	20	9.1
L1	L	1,000	83	650–800	27	13	9.0
M1	M	1,000	83	425–525	18	9	8.9
Sm1	S	1,000	83	300	10	5	8.7
AK64	Alaska M9.2 (1964)	650	280	no data	22.1	8.6	9.2
AKmax	Alaska Maximum	600	100	no data	30	no data	9.2

[a] Equivalent fault width calculated from rupture area divided by length; modeled fault width varies with latitude; Cascadia values (Sm1–XXL1) are from Witter and others (2011).

[b] Maximum slip estimates for Cascadia scenarios (Sm1–XXL1) are calculated from the recurrence interval multiplied by a convergence rate in southern Oregon (34 mm yr^{-1} at 42.94°W latitude) and are from Witter and others (2011); estimates for AK64 and AKmax are derived from the maximum subfault slip of Johnson and others (1996) and TPSW (2006), respectively.

[c] Average slip estimate is 0.49 of maximum slip estimate for Cascadia scenarios (XXL1–Sm1) and is from Witter and others (2011); estimates for AK64 and AKmax are from Johnson and others (1996) and TPSW (2006), respectively.

[d] Moment magnitude (M_w) = (log M_0 – 9.1)/1.5 where M_0 = seismic moment assuming rigidity = 4 × 1010 N m^{-2} and is from Witter and others (2011).

Table 2. Maximum coseismic uplift and subsidence, tsunami wave elevation, and percent confidence that Cascadia inundation scenarios cover all Cascadia inundation.

Rupture Scenario (Witter and others, 2011)	Tsunami Inundation Map (TIM Series) Scenario	Maximum Offshore Uplift (m)[a]	Maximum Offshore Subsidence[a] (m)	Maximum[b] Elevation at Nye Beach (MHHW, m)	Confidence[c] All Cascadia Inundation Covered (%)
XXL1	XXL	10.2	6.3	22.2	100
XL1	XL	9.2	5.6	21.2	98
L1	L	5.8	3.5	14.6	95
M1	M	3.8	2.4	9.9	79
SM1	S	2.6	1.6	6.1	26
AK64	Alaska M9.2 (1964)	8	4.5	2.7	na
AKmax	Alaska Maximum	13	6	6.1	na

[a] Cascadia values (Sm1–XXL1) are from Witter and others (2011).

[b] Observation point for wave elevation above model tide of mean higher high water (MHHW) is at longitude −124.06517° W, latitude 44.63864° N, 0 m NAVD88 at Nye Beach, Newport, Oregon; tsunami elevations in other areas will vary by large amounts from these values owing mainly to bathymetric effects, although there are also small latitudinal differences in Cascadia sources.

[c] Percent confidence limits are from Witter and others (2011) using 15 Cascadia tsunami simulations in the Bandon, Oregon, area and are derived from a logic tree considering only the sources of variability considered in that study; na is not applicable.

Table 3. Computational grids and input parameters for tsunami simulations. See Figure 3 for location of project areas and computational grids.

Tsunami Simulation Project Area	Number of Computational Grids[a]	Computational Grid Labels for Coastal Areas of High Refinement[b]	Assumed MHHW Tide (m NAVD88)	Tide Gauge[c]	Sponge Layer?[d]	Δt[e] (sec) Cascadia, Alaska	n_0[f] AKmax-AK64
Clatsop	2	A, B	2.71	Astoria	yes	2, 1	0.000
Tillamook	2	Neh+Nes, Till+Netz	2.536	Garibaldi	yes	2, 1	0.025
Central Coast	3	A, B, C	2.317	South Beach	yes	2, 0.5	0.000
Coos Bay	2	Coos Bay	2.07	Port Orford	no	2, 1	0.025
Bandon	2	Bandon	2.07	Port Orford	no	2, 1	0.025
South Coast	2	Gold Beach	2.07	Port Orford	no	2, 1	0.025

[a] Each project area in Figure 3 has multiple computational grids in order to limit the number of computational points in each computer run. For the Coos Bay, Bandon, and South Coast projects, there are two separate grids, one for Cascadia sources and one for Gulf of Alaska sources; the two grids differ only in degree of refinement in earthquake source areas; for the other project areas, high refinement is present for both the Alaska and Cascadia source areas for all grids, but refinement at the coast changes at the boundaries in Figure 3 (dashed lines).

[b] Letter names A, B, C are in order from north to south; Neh+Nes = Nehalem and Neskowin; Till+Netz = Tillamook Bay and Netarts Bay. Each area of high coastal refinement was incorporated into Cascadia and Alaska computational grids; the simulation results were then used to define inundation boundaries for the tsunami inundation maps (TIM series).

[c] Name of tide gauge in NOAA database (http://tidesandcurrents.noaa.gov/gmap3/) used to establish mean higher high water (MHHW).

[d] Sponge layers absorb outgoing wave energy, preventing wave reflections from domain boundaries into the domain.

[e] Δt = time step for simulations; 2 sec was optimal from convergence studies of Cascadia tsunamis and 0.5–1 sec for match to field observations of the 1964 Alaska tsunami.

[f] n_0 = Manning's coefficient, which was set to zero (zero friction) except as noted in the table for some AKmax and AK64 simulations.

CASCADIA EARTHQUAKE SOURCE MODEL

The CSZ earthquake scenarios developed here specify time intervals over which the maximum amount of coseismic slip accumulates (creating a "slip deficit") and is then released during long (>800 km) ruptures of the subduction zone megathrust. Calculations of maximum coseismic slip on the CSZ multiply representative time intervals over which slip deficit accumulates multiplied by a North American-Juan de Fuca plate convergence rate that varies with latitude according to the model of Wang and others (2003). Scenario slip deficit time intervals are chosen to be representative of time intervals between 19 turbidites (T1–T18) correlated along more than 800 km of the Cascadia margin (Witter and others, 2011; Goldfinger and others, 2012). Turbidites are submarine sand and silt slurries that appear to have been triggered by great Cascadia earthquakes over the last 10,000 years (Goldfinger and others, 2012). The intervals between offshore turbidite deposits range from as little as ~110 years to as long as ~1,150 years for deposits extending the full or nearly full length of the CSZ (Witter and others, 2011; Goldfinger and others, 2012). Vertical uplift and subsidence caused by each scenario fault rupture are simulated by integrating the point source dislocation solution of Okada (1985) over the 3D Cascadia megathrust assuming a uniform elastic half-space with a Poisson's ratio of 0.25 (see Witter and others [2011] for details).

Slip deficit time intervals were used to calculate peak slip for four general earthquake size classes labeled with "T-shirt" sizes: small (SM = 300 yrs), medium (M = 525 yrs), large (L = 800 yrs) and extra-large (XL=1,200 yrs). Slip was also progressively decreased by 12 to 19 percent from these values southward of the Columbia River to account for slip deficit reduced by additional smaller CSZ events inferred from turbidites that do not extend northward over the entire margin, as follows: M = 425–525 yrs, L = 650–800 yrs, and XL = 1,050–1,200 yrs. The maximum-considered event is an extra-extra-large (XXL) CSZ earthquake with no north-to-south tapering of slip (i.e., 1,200 yrs of slip deficit is released everywhere). No tapering of slip was also used for the SM scenario, as developing a separate source model for a north-to-south decrease of only 25 years of slip deficit was not considered cost effective. These earthquake size classes are inferred from systematic variations in turbidite mass that possibly reflect the strength and duration of shaking and from the time interval following the event. Positive correlation between turbidite mass and the time interval following many of the full-margin events in northern Cascadia implies that at least some full ruptures of the CSZ follow a quasi-time predictable behavior (Goldfinger and others, 2012), though longer-term cycling may also be in operation (Goldfinger and others, 2013). These observations led Goldfinger and others (2012) to infer that larger turbidites generally reflect larger earthquakes in the Holocene Cascadia record. The coseismic slip estimates inferred here are intended to encompass the range of plausible Cascadia earthquake rupture scenarios and do not represent predictions of the amount or distribution of slip likely to be released during a future event. See Witter and others (2011) for details.

Coseismic slip is released in a roughly "bell shaped" slip distribution, decreasing up and down dip on the subduction zone, the peak slip centered approximately beneath the top of the continental slope (Priest and others [2009, 2010]). Witter and others (2011) examined three different ways that the five scenario earthquakes could partition the bell-shaped slip distribution. Two placed the slip entirely on the megathrust, and one partitioned all of the slip onto a splay fault inclined ~30° landward (Figure 1; see Priest and others [2009] and Witter and others [2011] for evidence of the splay fault). They used a logic tree approach (Figure 2) to calculate likelihood of each scenario and the percent confidence that each scenario covered the possible variability. The splay fault scenarios created the largest tsunamis and were thus chosen for representation on the TIMs. They, in effect, also partially account for the amplifying effect of possible large trench-breaching slip that is not directly modeled in these scenarios but was recently observed in the Tōhoku earthquake of 2011 (e.g., Maeda and others, 2011). The splay fault scenarios had the following confidence levels: SM1 = 25%, M1=79%, L1 = 95%, XL1 = 98%, and XXL1 = 100% (Table 2). M1 had the highest logic tree weight (likelihood) overall. TIM map explanations label these scenarios S, M, L, XL, and XXL.

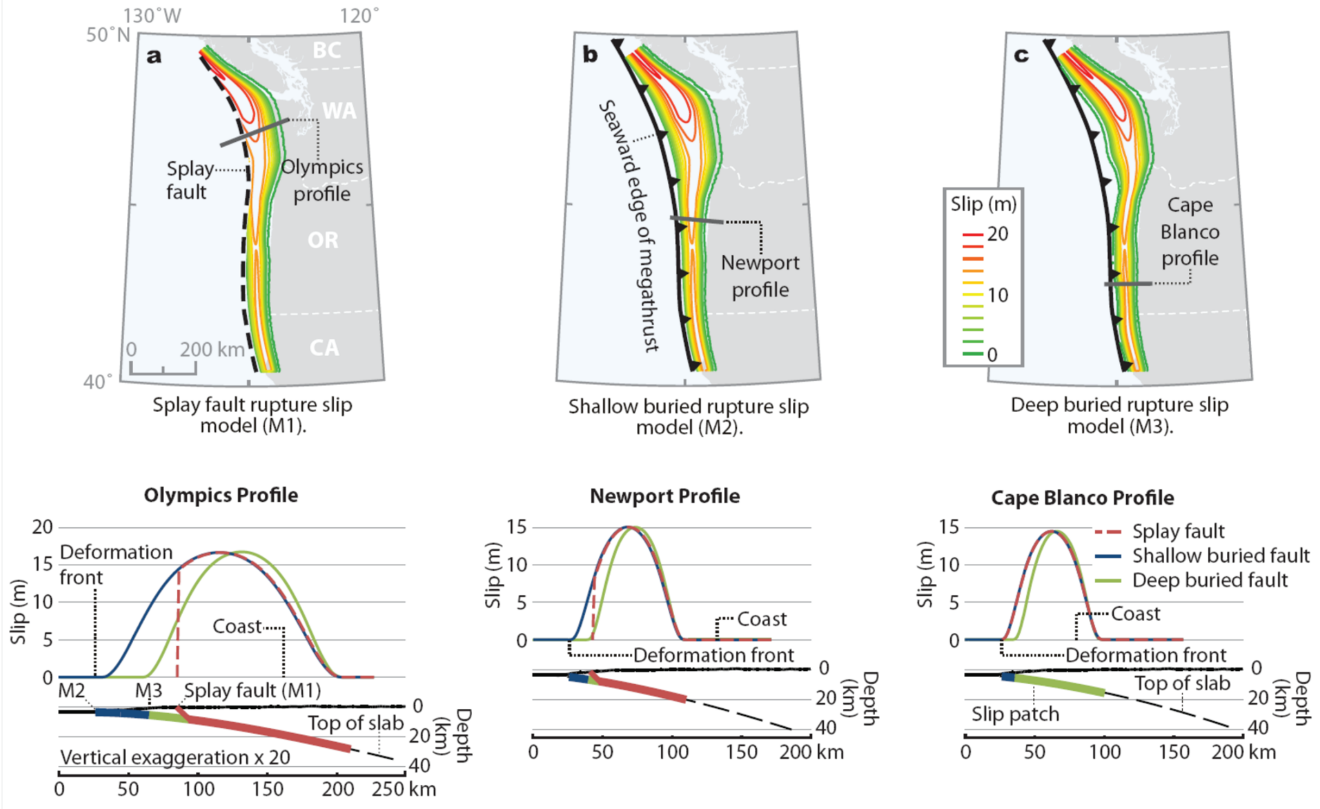

Figure 1. (top) Examples of earthquake rupture models using 425 to 525 years of slip employed in Cascadia tsunami simulations of "M" scenarios. (a) Splay fault rupture model for the M1 scenario; dashed line delineates splay fault. (b) Shallow buried rupture model (M2) where the updip limit of slip is at the deformation front. (c) Deep buried rupture deformation model (M3) where the updip limit of rupture is located east of the deformation front where the boundary between the inner and outer wedge is defined by landward vergent structures. (bottom) Profiles of fault slip for each model at three locations along the margin: the Olympic Peninsula, Washington; Newport, Oregon; and Cape Blanco, Oregon. Slip profiles are plotted as follows: M1 scenario, red; M2 scenario, blue; M3 scenario, green. Note that the model splay fault merges with the seaward edge of the Cascadia megathrust in southern Oregon and northern California. Slip patches for each fault model use the same color scheme and extend to same downdip limit. Taken from Witter and others (2011).

Figure 2. Schematic logic tree used by Witter and others (2011) to rank 15 Cascadia earthquake models. See Table 3 of Witter and others (2011) for a list of all parameters and weights used in the analysis. Earthquakes sizes are extra extra large (XXL), large (XL), large (L), medium (M), and small (SM). Figure is modified from Witter and others (2011) by correcting the slip deficit time for the SM branch to the value 300 and replacing the title "interevent time" with "slip deficit time."

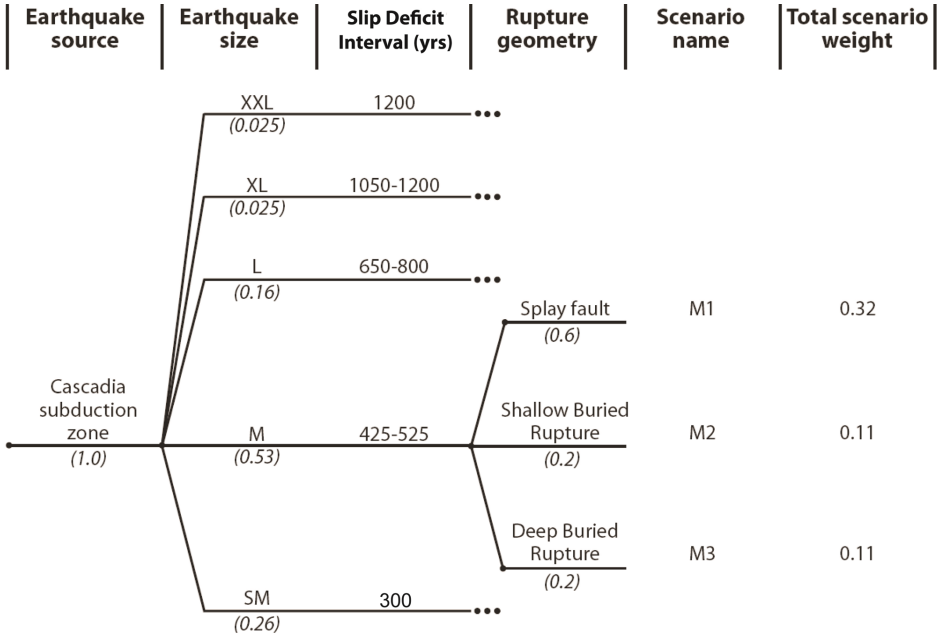

DISTANT TSUNAMI SOURCES

Sources for maximum-considered distant tsunamis are two M_w ~9.2 Gulf of Alaska earthquakes (Priest and others, 2009; Witter and others, 2011). The historical maximum event, AK64, replicates the 1964 Prince William Sound earthquake, which generated the largest distant tsunami to reach the Oregon coast in written history of North America. Vertical seafloor deformation was estimated from joint inversions of tsunami and geodetic data by Johnson and others (1996) and was used for the initial condition (earthquake-deformed sea surface) in the tsunami simulation. Simulations of this event were checked against 1964 observations of water levels and wave runup along the Oregon coast, allowing verification of the hydrodynamic model (see Priest and others [2009, 2010] for an example at Cannon Beach).

The hypothetical maximum-considered event, AKMax, is a Gulf of Alaska earthquake identified as "Source 3" in Table 1 of TPSW (2006). Their fault model has uniform slip on 12 subfaults with each subfault assigned an individual slip value of 15, 20, 25, or 30 m. These extreme parameters result in maximum seafloor uplift nearly twice as large as uplift produced by the 1964 earthquake as estimated by Johnson and others (1996). Analyses of the maximum tsunami amplitude simulated for this source show beams of higher energy more efficiently directed toward the Oregon coast compared with other Alaska-Aleutian subduction zone sources (TPSW, 2006). Because of its precedent use for the Seaside tsunami study by TPSW (2006), the hypothetical Gulf of Alaska scenario was used as a maximum-considered distant tsunami source; however, testing the geological plausibility of the scenario and the possibility of other sources with better directivity toward the coast south of Seaside was beyond the scope of the Witter and others (2011) and Priest and others (2009, 2010) studies.

NUMERICAL MODEL OF TSUNAMI WAVE PROPAGATION AND INUNDATION

The hydrodynamic model SELFE

Tsunami simulations use the hydrodynamic model SELFE (Zhang and Baptista, 2008)—the Semi-implicit Eulerian-Lagrangian Finite Element model used for cross-scale ocean circulation modeling, tsunamis, and storm surges. Algorithms used to solve the Navier-Stokes equations are computationally efficient and stable (Zhang and Baptista, 2008). Computational grids for simulations were constructed by first compiling a digital elevation model (DEM) covering the project area and then retrieving from the DEM elevations at a series of points defining a triangular irregular network (TIN) used as the computational grid. Grid spacing in the TIN differed from the detailed DEM in order to minimize computing time while accurately simulating geomorphic features controlling tsunami propagation and inundation (i.e., jetties, breakwaters, channels, and abrupt changes in slope). The final 13 computational grids (Table 3) had on the order of 1.4–5.6 million nodes with finest resolution at ~1 m. The grid size for the nearshore region (with depth 1 km or less) is chosen in such a way that the Courant-Friedrichs-Lewy (CFL) number is larger than 0.2 in order to avoid excessive numerical diffusion (Zhang and others, 2011). Resolution of <15 m was used in estuarine and river channels. Resolution in the most densely populated areas was <10 m (generally, 5 to 7 m). Grid spacing was adjusted so that at least five elements simulated the width of jetties and breakwaters. Unpopulated rural land areas without critical geomorphic features such as river channels had grid spacing up to 50 m. In the offshore, grid spacing increased smoothly with water depth, becoming ~1–5 km at abyssal depths. Earthquake source areas AKmax and AK64 had grid spacing of 2-3 km, while Cascadia source areas had spacing of ~0.6 km proximal to the project areas. In the earlier projects, on the southern coast, simulations for Alaska and Cascadia sources were run on two different grids differing only in degree of refinement at the source. Because the total number of grid points at the sources is a very small fraction of the grid, this approach was abandoned in the later northern and central coast simulations in favor of grids with the same refinement at both Alaska and Cascadia sources.

Because SELFE was used in the 2D mode, the Manning formulation was used in the bottom-friction calculation. To build in conservatism in the final inundation maps, a frictionless bottom (i.e. with Manning's $n_0 = 0$) was used for all CSZ scenarios and for the Central Coast and Clatsop County simulations of AK64 and AKmax. The earlier Bandon and South Coast simulations of AK64 and AKmax used a Manning's n_0 of 0.025. Zero friction was used in Central Coast and Clatsop County simulations of AK64 and AKmax in an effort to compensate for the omission of

nonlinear tidal interactions, which become important for smaller tsunamis in estuaries (e.g., Zhang and others 2011). This change was the result of testing simulations of AK64 against observations of 1964 inundations and flow depths in estuaries. As a result, there is slightly more inundation for equivalent Alaska scenarios in the central and northern Oregon TIMs than in the southern Oregon TIMs.

For the Clatsop, Tillamook, and Central Coast project areas (Figure 3), a sponge layer zone was applied near the ocean boundary to effectively absorb the outgoing wave energy; this was found to be particularly important for the larger CSZ scenarios with larger and persistent waves. The sponge layer technique prevents waves reflected by the computational domain boundary from contaminating the interior of the domain. This technique was not used in the Coos Bay, Bandon, or South Coast projects (Figure 3), but a sensitivity run for Coos Bay indicated that those results should not be affected. The time step (Δt) was 0.5–1 sec for the AK64 and AKmax simulations and 2 seconds for Cascadia simulations (Table 3). Time steps were set at the maximum values (shortest run times) while still producing accurate results, as determined by testing computational grids against field observations in the case of AK64, and by convergence study for Cascadia simulations.

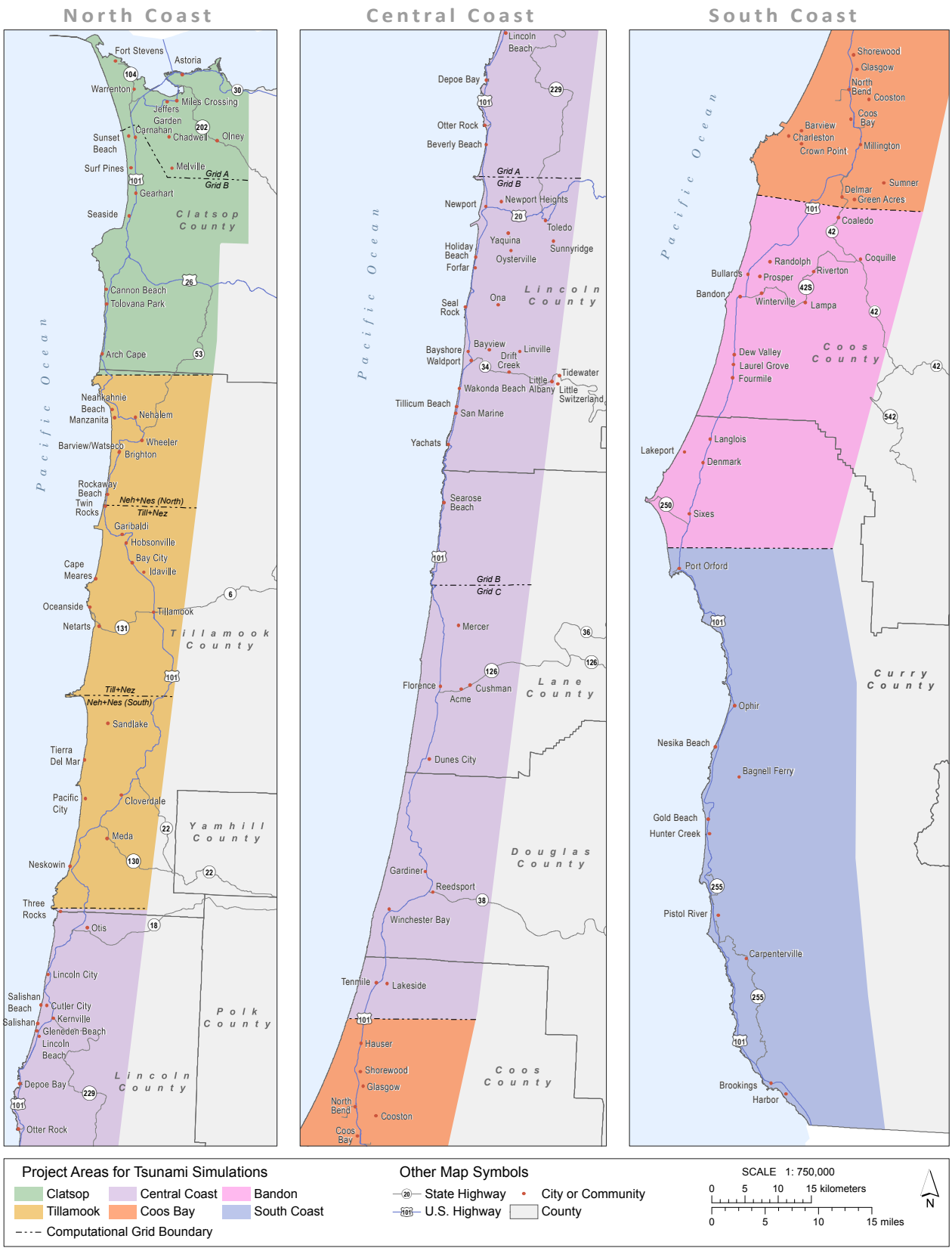

Figure 3. Tsunami project areas in Oregon showing boundaries of 11 separate areas of high computational grid refinement (black dashed lines) used to define Oregon tsunami inundation map (TIM series) inundations.

Bathymetric and topographic data for the DEM

Surface topography was primarily from DOGAMI 2008 light detection and ranging (lidar) data supplemented by U.S. Geological Survey (USGS) 10-m data where lidar data were unavailable. Nearshore bathymetry data were from the U.S. Army Corps of Engineers (USACE) supplemented by custom bathymetric surveys of some bays and estuaries (Nestucca Bay, Yaquina Bay, Alsea Bay, and the Siuslaw estuary). In addition, bathymetric data of Johnson and others (1985) for significant coastal lakes was used for lakes located in the inundation zone. In estuarine areas without either lidar or other bathymetric data, professional judgment was used to estimate potential water depths from adjacent bathymetric data. In these data gaps, a default depth of 3 m was assumed below the lidar-defined estuarine water elevation with smoothing between this depth and adjacent measured depths; Figure 4 illustrates some of the problems that had to be overcome when fusing differing data sets to depths inferred below lidar water surfaces from different flights. At Tillamook Bay where tidal channels were obvious on aerial photography but no bathymetry was available, the 3-m default depth was increased by ~2.5 m in order to simulate channels that could funnel tsunami energy. Pacific Ocean bathymetry outside of the USACE surveys was compiled from the ETOPO1 1-arc-minute database (http://www.ngdc.noaa.gov/mgg/global/global.html), 1/3-arc-second DEM data (http://www.ngdc.noaa.gov/dem/squareCellGrid/search), and, in a few parts of Tillamook County, by coastal DEMs (http://www.ngdc.noaa.gov/mgg/coastal/startcrm.htm) from the National Geophysical Data Center. All data sets were adjusted to the NAVD88 vertical datum and WGS84 map projection.

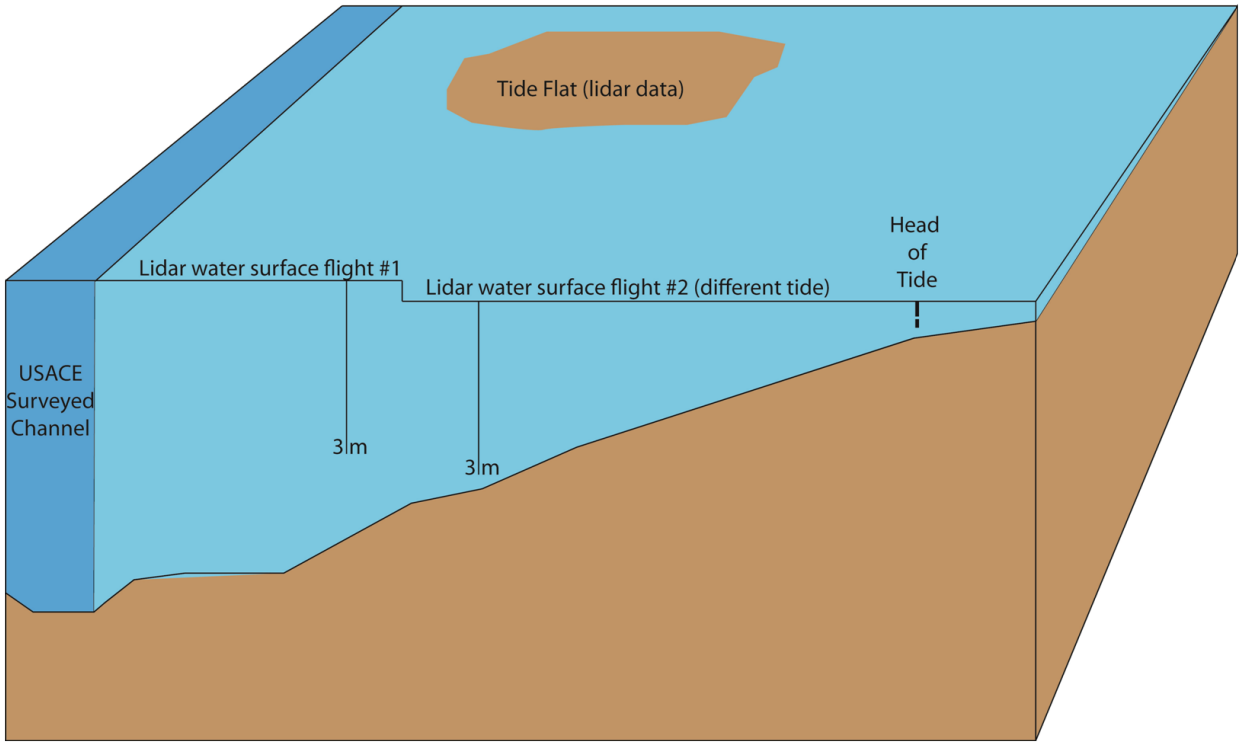

Figure 4. Illustration of fusing differing data sets into one digital elevation model (DEM). A default depth of 3 m below the lidar-defined water surface was assumed where no lidar or surveyed bathymetry was available, but in some areas lidar was flown at differing tides, creating steps in the inferred water depth that had to be removed. Smoothing was also needed above reach of highest tides where water depth was in many cases much less than 3 m. USACE = U.S. Army Corps of Engineers bathymetric data.

Tides

All tsunami simulations were run assuming that prevailing tide was static (no flow) and equal to mean higher high water (MHHW) at the nearest tide gauge station. Table 3 summarizes model tides for each computational grid of Figure 3.

GIS conversion

All tsunami scenarios were provided as ASCII text files to GIS analysts, who then used a GIS model to import the data into Esri file geodatabases. The model created several output files for each scenario including a master point feature class, a terrain feature class, and a contour line connecting the most landward wet nodes (wet contour) and the most landward dry nodes (dry contour). Interpretation and discretion were required to edit the lines for small island and pond features. These procedures are detailed in the appendix. Each scenario dry contour line was edited to correct vertices that lay landward of the next larger scenario. After all contour lines had been thoroughly quality checked and edited, they were used to create the wet/dry zone shown on the TIMs. This transition zone between wet and dry nodes equates to the amount of uncertainty in the model when determining the maximum inundation for each scenario.

The inundation polygons were created conservatively and extend to the landward dry nodes (dry contour). Additional vector lines were drawn 180 degrees into the ocean from the most northern and southern dry contour vertex and then connected. These lines were then converted to a polygon to create the final inundation zone.

All project area computational grids shown in Figure 3 contain areas of overlap. This figure shows not the actual grid extent but the location where the grids were seamed together (spliced) to form a cohesive polygon. The splice locality optimized precision of the overlapping simulations, using results from the most refined computational grid. The shapefile delineating these splice lines (Tsunami_Data_GridSeams) is included in this publication.

SHAPEFILES INCLUDED WITH THIS PUBLICATION

The following GIS shapefiles are included on the publication CD-ROM. Metadata is embedded in the shapefiles.

EvacuationBrochure_Data folder:
Assembly_Areas
CriticalFacilities
EvacuationZones
OutsideHazardArea_GreenHighGround

Reference_Files folder:
Evacuation_Brochure_Index_Polygons
TIM_Index_Polygons
Tsunami_Data_GridSeams

Statewide_Tsunami_Scenarios folder:
Statewide_AK64_Tsunami_Inundation_Scenario
Statewide_AKMAX_Tsunami_Inundation_Scenario
Statewide_L_Tsunami_Inundation_Scenario
Statewide_M_Tsunami_Inundation_Scenario
Statewide_SM_Tsunami_Inundation_Scenario
Statewide_XL_Tsunami_Inundation_Scenario
Statewide_XXL_Tsunami_Inundation_Scenario

REFERENCES

Goldfinger, C., Nelson, C. H., Morey, A., Johnson, J. E., Gutierrez-Pastor, J., Eriksson, A. T., Karabanov, E., Patton, J., Gracia, E., Enkin, R., Dallimore, A., Dunhill, G., and Vallier, T., 2012, Turbidite event history: methods and implications for Holocene paleoseismicity of the Cascadia subduction zone: Reston, Va., U.S. Geological Survey Professional Paper 1661-F, 178 p., 64 figures.

Goldfinger, C., Ikeda, Y., Yeats, R. S., and Ren, J., 2013, Superquakes and supercycles: Seismological Research Letters, v. 84, no. 1, p. 24–32.

Johnson, D. M., Petersen, R. R., Lycan, D. R., Sweet, J. W., and Neuhaus, M. E., 1985, Atlas of Oregon lakes: Corvallis, Oreg., Oregon State University Press, 322 p.

Johnson, J., Satake, K., Holdahl, S., and Sauber, J., 1996, The 1964 Prince William Sound earthquake: joint inversion of tsunami and geodetic data: J. Geophys. Res., v. 101, no. B1, p. 523–532.

Maeda, T., Furumaura, T., Shin'icki, S., and Shinohara, M., 2011, Significant tsunami observed at ocean-bottom pressure gauges during the 2011 off the Pacific coast of Tohoku earthquake: Earth Planets Space, v. 63, p. 803–808.

Okada, Y., 1985, Surface deformation due to shear and tensile faults in a half-space: Bull. Seismol. Soc. Am., v. 75, no. 4, p. 1135–1154.

Priest, G. R., Goldfinger, C., Wang, K., Witter, R., Zhang, Y., and Baptista, A. M., 2009, Tsunami hazard assessment of the Northern Oregon coast: a multi-deterministic approach tested at Cannon Beach, Clatsop County, Oregon. Oregon Department of Geology Mineral Industries Special Paper 41, 87 p.

Priest, G. R., Goldfinger, C., Wang, K., Witter, R., Zhang, Y., and Baptista, A. M., 2010, Confidence levels for tsunami-inundation limits in northern Oregon inferred from a 10,000-year history of great earthquakes at the Cascadia subduction zone: Natural Hazards, doi:10.1007/s11069-009-9453-5.

Tsunami Pilot Study Working Group (TPSW), 2006, Seaside, Oregon tsunami pilot study—modernization of FEMA flood hazard maps: Seattle, Wash., National Oceanic and Atmospheric Administration, OAR Special Report, NOAA/OAR/PMEL.

Wang, K, R. Wells, S. Mazzotti, R. D. Hyndman, and T. Sagiya, 2003, A revised dislocation model of interseismic deformation of the Cascadia subduction zone, Journal of Geophysical Research, v. 108, no. B1, p. 2009, doi:10.1029/2001JB001227.

Witter, R. C., Zhang, Y. J., Wang, K., Priest, G. R., Goldfinger, C., Stimely, L., English, J. T., and Ferro, P. A., 2011, Simulating tsunami inundation at Bandon, Coos County, Oregon, using hypothetical Cascadia and Alaska earthquake scenarios: Oregon Department of Geology Mineral Industries Special Paper 43, 57 p.

Zhang, Y., and Baptista, A. M., 2008, An efficient and robust tsunami model on unstructured grids; Part I, inundation benchmarks: Pure and Applied Geophysics, v. 165, no. 11-12, p. 2229–2248.

Zhang, Y., Witter, R. W., and Priest, G. P., 2011, Tsunami-tide interaction in 1964 Prince William Sound Tsunami: Ocean Modelling, v. 40, 246–259.

APPENDIX: ASSUMPTIONS AND CRITERIA USED TO INTERPRET AND SIMPLIFY INUNDATION LINES

The varying resolution of the unstructured grid resulted in a complicated collection of lines including one continuous line marking the general extent of maximum inundation along the coast as well as numerous islands and ponds. “Islands” are dry regions within the inundated area; “ponds” are wet regions outside the inundation area (Figure A1). The primary parameter used to determine significance was size. Dimensions were measured from one dry edge to the other, which resulted in measuring the "inside" dimensions for islands and the "outside" dimensions for ponds. Any area with a smallest dimension of less than five computational nodes was considered to be poorly defined by the simulation and was generally not depicted on published maps. This rule was most strictly followed when drawing inundation lines for the Central Coast and Clatsop projects (Figure 3); for the other projects minimum dimensions were used to edit out extraneous inundation polygons. (See explanations of these dimensions below.) In addition, judgment was required with regard to the physical setting of the feature. For example, some “ponds” had no possible hydraulic connection to the tsunami or waterways but were wetted by the simulation because they were considered below tide after coseismic subsidence. Dry “islands” of easily eroded dune sand near the minimum size threshold were generally eliminated.

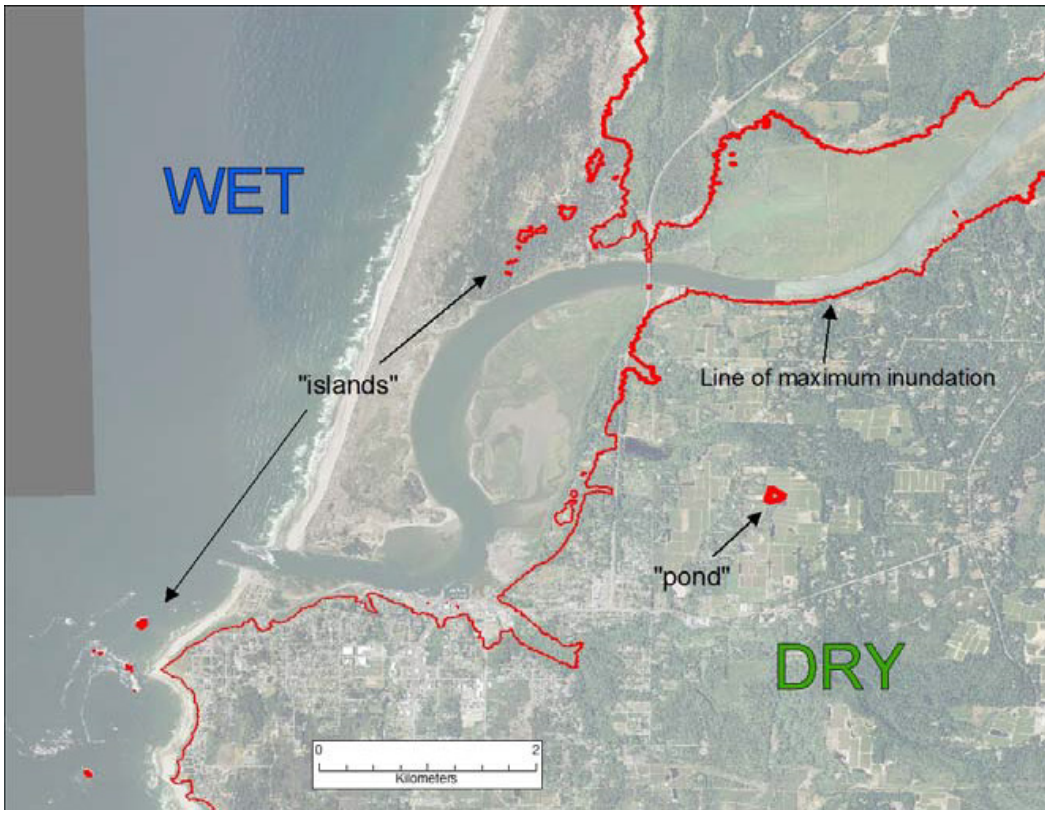

Figure A1. Example of a line of maximum tsunami inundation including the single continuous line as well as “islands” and “ponds,” anomalous wet and dry regions that occur throughout the study area.

Islands

Islands include both linear and nonlinear map features. Linear features such as dunes and levees may or may not be completely captured by the unstructured grid depending on grid resolution. Significant linear features included on the map were defined as being greater than 300 m long and greater than 50 m wide. Features with smaller dimensions are not included on the published map. Figure A2 shows examples of levees and dunes within the Bandon study area.

Nonlinear "island" features include sea stacks and some headlands (Figure A3). Significant nonlinear "Island" features were defined as being greater than 300 m wide by 200 m long. Smaller islands were not included in the published map.

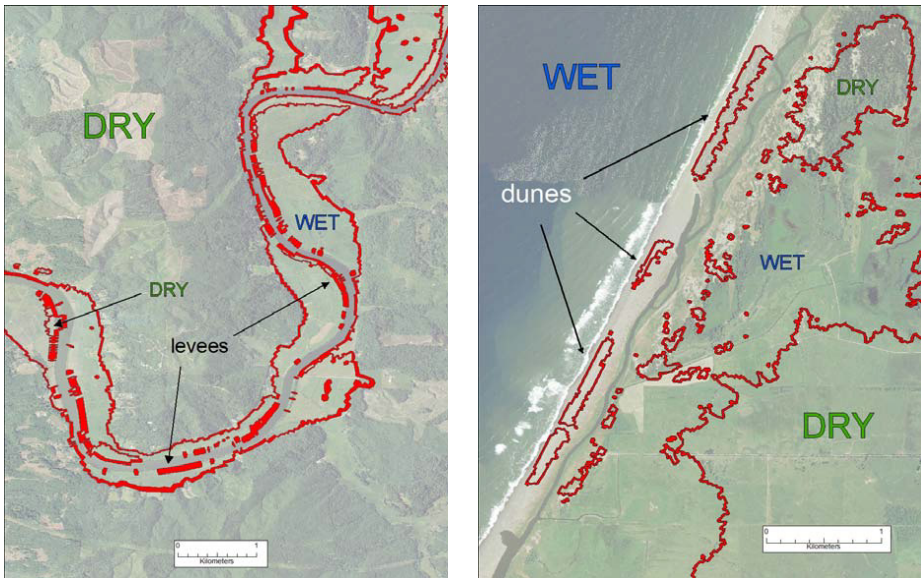

Figure A2. Examples of levee and dune "islands." Significant linear features were defined as being greater than 300 m long and greater than 50 m wide.

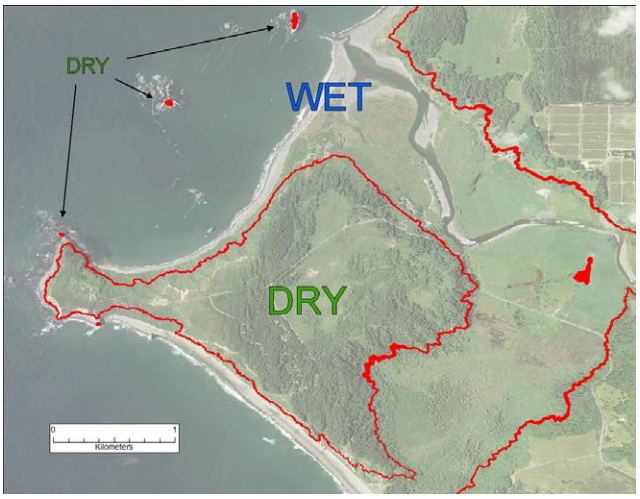

Figure A3. In this example, the island defined by the Cape Blanco headland was included on the map, whereas the sea stacks were considered insignificant and were not included on the map.

Ponds

Wet areas outside the extent of the main inundation area are referred to as "ponds." These are predominantly areas that subside during the earthquake and reside below the tidal datum used in the model (MHHW). Most are nonlinear in shape with the exception of rare linear or sinuous tidal sloughs or secondary river channels. Significant pond features included in the map were at least 300 m by 200 m; smaller features were overlooked. Channels are the other primary "pond" feature, as they can efficiently carry tsunami wave energy significantly upstream of the main inundation extent. Main stem channels of rivers, regardless of width, were considered significant and included on the map. Occasionally, there was clear evidence of hydraulic connectivity (interpreted from aerial photographs and/or lidar), but the model produced a disconnect (due to grid resolution), such as a gap in a contiguous river or tidal channel (Figure A4a) or a complicated relationship between the main inundation line and adjacent "ponds" (Figure A5a). Gaps in a channel were connected by hand (Figure A4b) and the aforementioned complicated relationships were simplified by hand (Figure A5b).

Exceptions to the rules

In residential areas and parks, if there are islands that are closer to the inhabitants than the nearest edge of the evacuation zone, we may choose to include them. We may also modify a polygon when the model predicts a dry zone over a body of water.

(a) Initial inundation line: (b) Interpreted line:

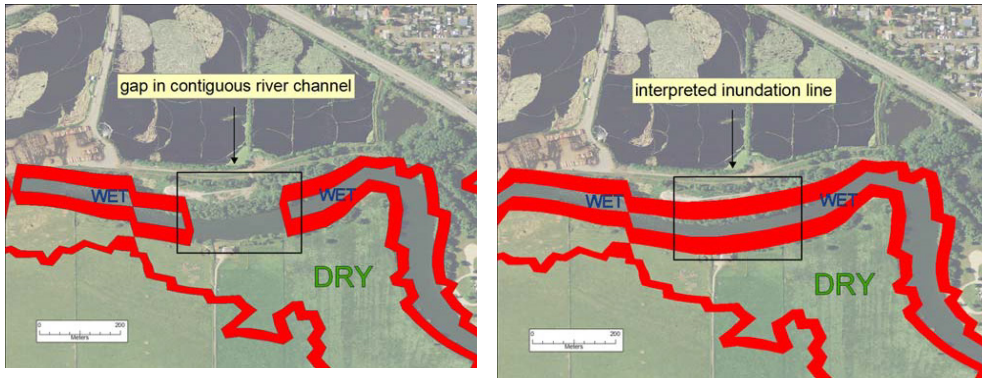

Figure A4. (a) Example of a gap in the maximum inundation line along the Coquille River and (b) the interpreted line showing a manual edit reconnecting the inundation line along the channel.

(a) Initial inundation line: (b) Interpreted line:

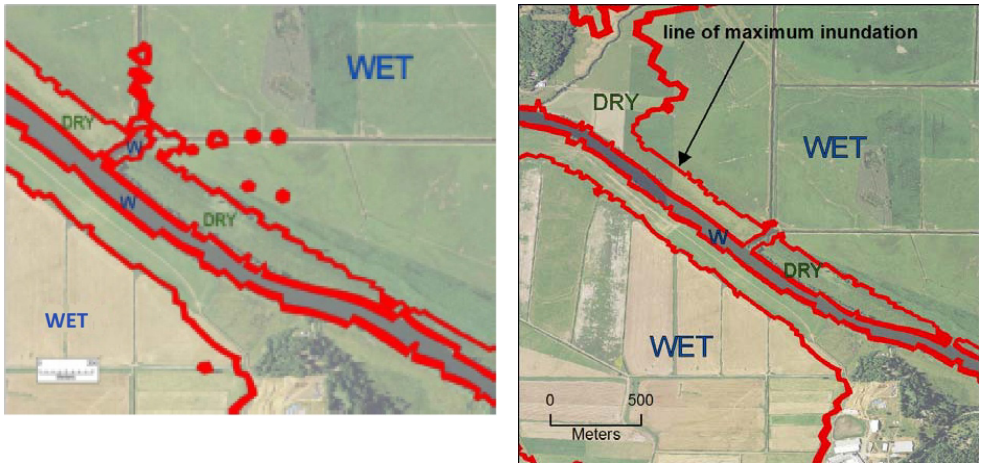

Figure A5. (a) Example of a complicated relationship between the main inundation line and adjacent "ponds" and (b) the interpreted simplification. This is low-lying pasture land adjacent to the Coquille River, west of Coquille, Oregon.